Macromolecules
ARTICLE

Macromolecules **2010**, *43*, 8209–8217 **8209**
DOI: 10.1021/ma101518a

Microphase Separation of High Grafting Density Asymmetric Mixed Homopolymer Brushes on Silica Particles

Xiaoming Jiang,[†] Bin Zhao,*[,†] Ganji Zhong,[‡,§] Naixiong Jin,[†] Jonathan M. Horton,[†] Lei Zhu,[‡] Robert S. Hafner,[∥] and Timothy P. Lodge[⊥]

[†]*Department of Chemistry, University of Tennessee, Knoxville, Tennessee 37996,* [‡]*Department of Macromolecular Science and Engineering, Case Western Reserve University, Cleveland, Ohio 44106,* [§]*College of Polymer Science and Engineering, Sichuan University, Chengdu 610065, People's Republic of China,* [∥]*The Characterization Facility of the College of Science and Engineering, University of Minnesota, Minneapolis, Minnesota 55455, and* [⊥]*Department of Chemistry, University of Minnesota, Minneapolis, Minnesota 55455*

Received July 7, 2010; Revised Manuscript Received September 4, 2010

ABSTRACT: A set of high grafting density mixed poly(*tert*-butyl acrylate) (P*t*BA)/polystyrene (PS) brushes with P*t*BA number-average molecular weight (M_n) fixed at 18.6 kDa and PS M_n ranging from 8.7 to 28.0 kDa was synthesized from 172 nm asymmetric difunctional initiator (Y-initiator)-functionalized silica particles by sequential surface-initiated atom transfer radical polymerization of *tert*-butyl acrylate and nitroxide-mediated radical polymerization (NMRP) of styrene. The Y-initiator-functionalized particles were prepared by the immobilization of a triethoxysilane-terminated Y-initiator onto the surface of bare silica particles via a hydrolysis/condensation process. The overall grafting densities of the obtained mixed brushes were 0.9−1.2 chains/nm^2, which were significantly higher than those of mixed brushes prepared from silica particles that were surface functionalized by a monochlorosilane-terminated Y-initiator (0.6−0.7 chains/nm^2). Differential scanning calorimetry analysis showed that all high density mixed brushes exhibited two distinct glass transitions, suggesting that the two grafted polymers were microphase separated in the brush layer. TEM showed that with the increase of PS M_n from 8.7 to 28.0 kDa the morphology of the mixed brushes changed from mostly isolated PS nanodomains buried in the P*t*BA matrix to a nearly cocontinuous nanostructure and two-layered nanostructures composed of a laterally microphase-separated bottom layer and a thin PS top layer. These morphologies were similar to the asymmetric mixed brushes with grafting densities of 0.6−0.7 chains/nm^2. However, the feature sizes of the patterns formed from the microphase separation were much smaller. The observed grafting density effect on the pattern feature size was further confirmed from the study of a high grafting density mixed brush sample with P*t*BA M_n of 23.7 kDa and PS M_n of 25.7 kDa.

Introduction

Mixed brushes, composed of two chemically distinct homopolymers each end-grafted on a solid substrate in a random or alternating fashion, are an intriguing class of surface-responsive materials.[1−4] Driven by free energy minimization, the two grafted polymers in the brush layer can undergo spontaneous chain reorganization in response to environmental variations. Consequently, mixed brushes exhibit different nanostructures and surface properties under different conditions. These brushes have attracted tremendous interest in the past two decades because of their rich phase behavior and potential in technological applications; their responsive properties have been intensively investigated both theoretically and experimentally.[1−10]

Marko and Witten predicted that under equilibrium melt conditions binary symmetric mixed homopolymer brushes on a flat substrate would undergo lateral microphase separation, yielding a "rippled" nanostructure.[1a] They pointed out that the transitions between different ordered states could be achieved by altering the component compositions and molecular weights. After this seminal work, the lateral microphase separation of symmetric mixed brushes under melt or near-melt conditions and in nonselective solvents were also observed in other theoretical and simulation studies.[1c,d,3−6] Moreover, the effects of various molecular parameters on the phase morphology of mixed brushes were investigated, and many interesting nanostructures have been predicted.

Of particular interest to the present work are the effects of chain length disparity and grafting density on the self-assembled nanostructures of mixed brushes.[3,4a,5,6] The effect of chain length disparity on phase morphology of mixed brushes has been theoretically investigated.[5,6] Using computer simulations, Roan studied the microphase separation of mixed brushes on spherical nanoparticles with a radius comparable to the $\langle R_{rms} \rangle$ values of grafted polymers and observed a variety of ordered nanostructures.[5] For instance, the equilibrium morphology evolves from a rippled, to a 12-islanded, and then a layered structure with the increase of chain length difference under the condition that the grafting densities of two polymers are identical. Wang and Müller recently used single-chain-in-mean-field simulation to investigate the phase behavior of asymmetric mixed brushes on flat substrates.[6] At a large chain length asymmetry, mixed brushes were found to self-assemble into a two-layered nanostructure in a nearly nonselective solvent: a laterally structured bottom layer and a top layer containing only the longer polymer species.[6] The effect of grafting density on microphase separation of mixed brushes has also been studied theoretically. In general, decreasing the grafting density leads to the weakening of the demixing interactions between two grafted polymers in the brush

*Corresponding author. E-mail: zhao@ion.chem.utk.edu.

Published on Web 09/17/2010

Scheme 1. Schematic Illustration for the Synthesis of High Grafting Density Mixed P*t*BA/PS Brushes with a Fixed P*t*BA M_n and Various PS Molecular Weights by Sequential Atom Transfer Radical Polymerization (ATRP) and Nitroxide-Mediated Radical Polymerization (NMRP) from Y-Initiator-Functionalized Silica Particles

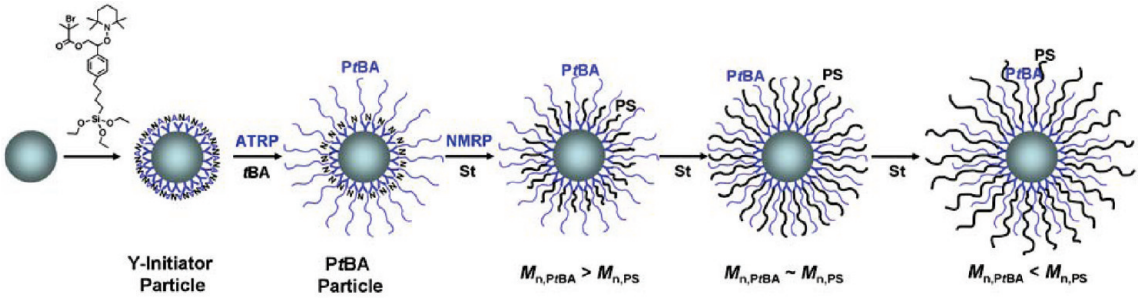

layer.[3] In the limit where the two polymers are highly incompatible and their grafting densities are high, Zhulina and Balazs found, by scaling arguments, that in nonselective poor solvents the periodicity of the ripple pattern scales with the one-sixth power of the area per chain;[3] i.e., the ripple wavelength decreases with increasing grafting density.

There have been a few experimental studies on asymmetric mixed brushes on flat substrates.[8c,9d] Minko et al. prepared a series of asymmetric mixed brushes by a "grafting to" method and investigated them by atomic force microscopy (AFM) and contact angle measurements.[8c] For a small chain length asymmetry, the brushes were found to exhibit lateral and vertical segregation, depending on the solvent quality. With the increase of molecular weight asymmetry, a transition from a "rippled" to a layered structure was observed. We previously synthesized mixed brushes with various chain length asymmetries from asymmetric difunctional initiator (Y-initiator)-functionalized silicon wafers by sequential surface-initiated atom transfer radical polymerization (ATRP) and nitroxide-mediated radical polymerization (NMRP) and studied their responsive properties upon exposure to different solvents by AFM, X-ray photoelectron spectroscopy, and contact angle measurements.[9d] Although interesting results have been obtained from these studies, the phase morphologies of asymmetric mixed brushes had not been directly visualized in these two works.

Transmission electron microscopy (TEM) allows for direct observation of phase morphologies of mixed brushes, provided that the samples are suitable for TEM experiments and are properly stained, if needed.[11,12] We recently reported the synthesis of a series of asymmetric mixed poly(*tert*-butyl acrylate) (P*t*BA)/polystyrene (PS) brushes by sequential ATRP of *t*BA and NMRP of styrene from 160 nm silica particles that were functionalized by a monochlorosilane-terminated Y-initiator.[13] The total grafting densities (σ_{total}) of these mixed brushes were 0.6−0.7 chains/nm^2 (these brushes are termed intermediate grafting density mixed brushes, IDMB). With the increase of PS M_n from below to above the M_n of P*t*BA, the morphology of mixed brushes evolved from isolated, nearly spherical PS nanodomains buried inside the P*t*BA matrix, to short PS cylinders, to nearly bicontinuous nanostructures, and a two-layered nanostructure composed of a laterally microphase-separated bottom layer and a thin PS top layer.

Although mixed brushes were intensively studied in recent years, few experimental investigations were directed to the effect of grafting density on phase morphology of mixed brushes. In the present work, we prepared a set of high grafting density asymmetric mixed P*t*BA/PS brushes (HDMB, σ_{total} = 0.9−1.2 chains/nm^2) and studied their phase behavior by using differential scanning calorimetry (DSC) and TEM. A triethoxysilane-terminated Y-initiator was synthesized and immobilized onto silica particles via a hydrolysis/condensation process (Scheme 1). This initiator immobilization method was first used by Ohno et al. for the synthesis of high grafting density homopolymer brushes on silica particles (σ = 0.65−0.9 chains/nm^2).[14] P*t*BA brushes were then grown first from Y-initiator particles by surface-initiated ATRP of *t*BA at 75 °C, followed by NMRP of styrene at 120 °C. The "living" nature[15] of NMRP allows for the synthesis of mixed brushes with various PS molecular weights in a one-pot reaction (Scheme 1). Their morphologies were compared with intermediate density mixed P*t*BA/PS brushes made from monochlorosilane-functionalized silica particles. We found that the feature sizes of the patterns formed from self-assembly of HDMB were significantly smaller than those from IDMB.

Results and Discussion

Synthesis of High Grafting Density Asymmetric Mixed P*t*BA/PS Brushes on Silica Particles. We used a procedure similar to that reported by Ohno et al.[14] to immobilize a triethoxysilane-containing Y-initiator (Scheme 1) onto bare silica particles.[16] The key to this method is the ammonia-catalyzed hydrolysis and condensation of the Y-initiator-terminated triethoxysilane on the surface of bare silica particles in ethanol, yielding a high density initiator layer. The results from Ohno et al. suggested that this method produced a uniform initiator layer on the surface of silica particles.[14] The bare silica particles were synthesized by the Stöber process, which is known to produce silica particles with a relatively uniform size distribution.[17] The triethoxysilane-containing Y-initiator was prepared by a platinum-catalyzed hydrosilylation reaction of 2-[4-(but-3-enyl)phenyl]-2-(2′,2′,6′,6′-tetramethyl-1′-piperidinyloxy)ethyl 2-bromo-2-methylpropanoate (the Y-silane precursor) with triethoxysilane (HSi(OC$_2$H$_5$)$_3$). After the immobilization reaction proceeded at 40 °C for 18 h, the particles were isolated by centrifugation and repeatedly washed with THF. The average diameter of the Y-initiator-functionalized silica particles (Y-initiator particles) was 172 nm, measured from TEM micrographs. Thermogravimetric analysis (TGA) showed that the weight loss of Y-initiator particles relative to bare silica particles was 4.4% when the weight retention difference at 100 °C between the two curves was taken into consideration (Figure 1).

The Y-initiator particles were then used for preparing mixed P*t*BA/PS brushes. P*t*BA was grown first by surface-initiated ATRP of *t*-butyl acrylate carried out in anisole at 75 °C using CuBr/*N*,*N*,*N*′,*N*′,*N*″-pentamethyldiethylenetriamine (PMDETA) as catalyst and ethyl 2-bromoisobutyrate (EBiB) as free initiator. The TEMPO group in the Y-initiator was previously confirmed to be stable under this ATRP condition.[9,18] The polymerization was stopped when the molecular weight of the free P*t*BA reached 18.6 kDa, determined by size exclusion chromatography (SEC). The polydispersity index (PDI) of this free polymer was 1.09, suggesting that the polymerization was controlled. The average

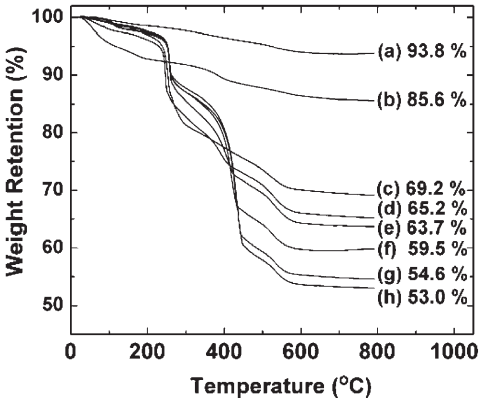

Figure 1. Thermogravimetric analysis (TGA) of (a) bare silica particles, (b) Y-initiator particles, (c) P*t*BA brush-grafted particles with P*t*BA M_n of 18.6 kDa, (d) mixed brush-grafted particles with P*t*BA M_n of 18.6 kDa and PS M_n of 8.7 kDa (particle **I-1**), (e) mixed brush-grafted particles with P*t*BA M_n of 18.6 kDa and PS M_n of 13.4 kDa (particle **I-2**), (f) mixed brush-grafted particles with P*t*BA M_n of 18.6 kDa and PS M_n of 19.4 kDa (particle **I-3**), (g) mixed brush-grafted particles with P*t*BA M_n of 18.6 kDa and PS M_n of 25.3 kDa (particle **I-4**), and (h) mixed brush-grafted particles with P*t*BA M_n of 18.6 kDa and PS M_n of 28.0 kDa (particle **I-5**). TGA was performed in air at a heating rate of 20 °C/min from room temperature to 800 °C.

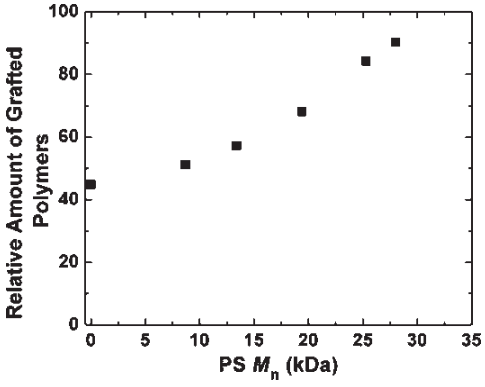

Figure 2. Amount of the grafted polymers in mixed P*t*BA/PS brush-grafted silica particles relative to the silica residue at 800 °C, calculated from TGA data, versus PS molecular weight.

degree of polymerization (DP) of the free polymer was 143, which was calculated from the monomer conversion, determined by ^{1}H NMR spectroscopy analysis, and the initial monomer-to-initiator ratio. It has been established that the molecular weight and molecular weight distribution of polymer brushes synthesized by surface-initiated "living"/controlled radical polymerization, including high density homopolymer brushes (with grafting density of 0.65−0.90 chains/nm^2),[14] are essentially identical to those of the free polymer formed from the free initiator.[9f,14,19] TGA showed that the weight retention of P*t*BA brush-grafted particles at ~800 °C was 69.2% (Figure 1). By using the average size of Y-initiator particles (172 nm), TGA data, and the DP of the free P*t*BA, and assuming that the density of silica particles was identical to bulk SiO_2 (2.07 g/cm^3),[9f] the grafting density of P*t*BA brushes on silica particles was calculated to be 0.63 chains/nm^2. This value was comparable to those of high density homopolymer brushes (σ = 0.65−0.90 chains/nm^2) on silica particles reported by Ohno et al.[14] and was significantly higher than that of P*t*BA brushes that were grown from monochlorosilane-terminated Y-initiator-functionalized silica particles (σ = 0.36 chains/nm^2).[13]

By taking advantage of the "living" nature of NMRP, a set of mixed P*t*BA/PS brush-grafted particle samples with PS molecular weights ranging from below to above the P*t*BA M_n were synthesized from P*t*BA brush-grafted particles in a one-pot reaction via surface-initiated NMRP of styrene. The polymerization was carried out in anisole at 120 °C, and a free initiator, 1-phenyl-1-(2′,2′,6′,6′-tetramethyl-1′-piperidinyloxy)-ethane (STEMPO), was added into the reaction mixture to facilitate the control of surface-initiated polymerization. Five mixed brush samples with the same P*t*BA M_n but different PS molecular weights were obtained at different polymerization times. The particles were isolated by centrifugation and repeatedly washed with THF. The free polymers were purified and analyzed by SEC.

SEC analysis of five free polymers showed that the molecular weight of PS increased smoothly with the increase of reaction time, while the PDI gradually decreased,[20] indicating that the polymerization was controlled. Specifically, the M_n of PS increased from 8.7 kDa (the corresponding hairy particles designated as particle **I-1**), to 13.4 kDa (the particles designated as particle **I-2**), to 19.4 kDa (the particles designated as particle **I-3**), to 25.3 kDa (the particles designated as particle **I-4**), and 28.0 kDa (the particles designated as particle **I-5**). Note that by cleaving the grafted polymers off silica particles and hydrolyzing the ester bond in the Y-initiator, we previously confirmed from SEC and ^{1}H NMR studies that the molecular weight and molecular weight distribution of the grafted PS were identical to those of the free PS.[9f] Considering this experimental observation and the aforementioned result for high density homopolymer brushes from Ohno et al.,[14] it is reasonable to assume that the values of M_n and PDI of the grafted PS in current asymmetric mixed brush samples are also the same as those of the free PS, though the grafting densities are higher. From Figure 1, the weight retention of mixed brush-grafted particles at 800 °C decreased with the increase of PS M_n, from 65.2% for particle **I-1**, to 63.7% for particle **I-2**, to 59.5% for particle **I-3**, 54.6% for particle **I-4**, and 53.0% for particle **I-5**. Using the silica residue at 800 °C as reference and taking into consideration the difference in weight retention at 100 °C between hairy particles and Y-initiator particles, we calculated the relative amount of the grafted polymers on silica particles in each sample and plotted it again the PS molecular weight (Figure 2). The amount of the grafted polymers increased with PS M_n; however, the increase was slow in the beginning of the polymerization. This seemed to be inherent to the TEMPO-mediated radical polymerization, as we previously also observed a slow period in the study of the kinetics of NMRP.[9f]

On the basis of the average size of Y-initiator particles (172 nm), the TGA data in Figure 1, and the PS M_n, we calculated the grafting density of PS in each sample. The results are summarized in Table 1. The total grafting densities of two polymers ($\sigma_{total} = \sigma_{PtBA} + \sigma_{PS}$) in these samples were in the range of 0.9−1.2 chains/nm^2. Except for the first two samples (particles **I-1** and **I-2**), the grafting densities of two polymers were reasonably close to each other. The lower PS grafting densities of particles **I-1** and **I-2** could be the result of the slow reaction period in the early stage of the polymerization.[9f] Calculations showed that the average distance between grafting sites in these mixed brush samples was 0.91−1.06 nm, indicating that the polymers were densely grafted and highly stretched. For comparison, we include in Table 1 four intermediate density mixed P*t*BA/PS brush samples with total grafting densities of 0.6−0.7 chains/nm^2 (particles **II-1** to **II-4**). These IDMB samples were synthesized from 160 nm silica particles that were functionalized by a monochlorosilane-terminated Y-initiator. The detailed synthesis

Table 1. Molecular Characteristics of Mixed P*t*BA/PS Brushes with Various P*t*BA and PS Molecular Weights on Silica Particles and the Corresponding Free Polymers

sample	PS M_n (kDa), PDI, DP[b]	DP_{PS}/DP_{PtBA}[c]	σ_{PS} and σ_{total} (chains/nm^2)[d]	$\langle R_{rms}\rangle$ (nm)[e]	typical PS domain width and periodicity (nm)[h]
particle **I-1**[a]	8.7, 1.28, 84	0.59	0.26, 0.89	6.2	8, NA
particle **I-2**[a]	13.4, 1.19, 129	0.90	0.33, 0.96	7.6	8, 12
particle **I-3**[a]	19.4, 1.14, 187	1.31	0.43, 1.06	9.2	8, 12
particle **I-4**[a]	25.3, 1.13, 243	1.70	0.56, 1.19	10.5	7, 11
particle **I-5**[a]	28.0, 1.11, 269	1.88	0.58, 1.21	11.0	6, 11
particle **II-1**[f]	14.8, 1.24, 142	0.74	0.21, 0.57	8.0	13, NA
particle **II-2**[f]	18.7, 1.20, 180	0.94	0.26, 0.62	9.0	13, NA
particle **II-3**[f]	24.9, 1.17, 239	1.25	0.27, 0.63	10.4	15, 20
particle **II-4**[f]	30.4, 1.14, 292	1.53	0.32, 0.68	11.5	17, 22
particle **III-1**[g]	25.7, 1.14, 247	1.31	0.51, 0.99	10.5	8, 13

[a] Particles **I-1** to **I-5** were prepared from P*t*BA brush-grafted silica particles with P*t*BA M_n of 18.6 kDa and PDI of 1.09; DP_{PtBA} = 143; the grafting density of P*t*BA (σ_{PtBA}) was 0.63 chains/nm^2. [b] The values of M_n and polydispersity index (PDI) of PS were determined by SEC; the DPs of PS were calculated from M_ns. [c] The ratio of DPs of two polymers. [d] The PS grafting density (σ_{PS}) in each sample was calculated using the size of Y-initiator particles, DP_{PS}, and TGA data. The total grafting density $\sigma_{total} = \sigma_{PtBA} + \sigma_{PS}$. [e] $\langle R_{rms}\rangle$ is root-mean-square end-to-end distance of polymer chains in the unperturbed state. The values of $\langle R_{rms}\rangle$ were calculated using $\langle R_{rms}\rangle = (C_\infty nl^2)^{1/2}$, where C_∞ is the Flory's characteristic ratio for an infinite chain, n the number of C−C bonds in the chain (n = 2DP), and l the bond length of C−C bond (1.54 Å).[21] The value of C_∞ for P*t*BA was not available in the literature. We used the value of C_∞ (9.5) of PS to estimate the $\langle R_{rms}\rangle$ of P*t*BA. The $\langle R_{rms}\rangle$s of P*t*BA with DPs of 143, 189, and 191 in the unperturbed state are 8.0, 9.2, and 9.2 nm, respectively. [f] Particles **II-1** to **II-4** were prepared from P*t*BA brush-grafted silica particles with P*t*BA M_n of 24.5 kDa and PDI of 1.11, which were prepared from 160 nm monochlorosilane-terminated Y-initiator-functionalized silica particles.[13] DP_{PtBA} = 191. The σ_{PtBA} was 0.36 chains/nm^2. [g] Particle **III-1** was prepared from P*t*BA brush-grafted silica particles with P*t*BA M_n of 23.7 kDa and PDI of 1.09;[16] the DP_{PtBA} was 189 and the σ_{PtBA} was 0.48 chains/nm^2. [h] The width of a typical PS nanodomain and the ripple wavelength were estimated from TEM micrographs.

and characterization can be found in a previous publication.[13] Clearly, the total grafting densities of mixed brushes in the particle **I** series were substantially higher than those in the particle **II** series. At a similar ratio of DP_{PS} to DP_{PtBA}, the σ_{total} for a sample in the particle **I** series was 1.5−1.8 times that for the corresponding sample in the particle **II** series.

DSC Study of High Density Mixed P*t*BA/PS Brush-Grafted Silica Particles. DSC has been widely used to study the phase behavior of multicomponent polymeric systems. We previously observed that there were two distinct glass transitions in the DSC thermogram for the microphase-separated mixed brushes on silica particles, while miscible mixed brushes exhibited only one broad glass transition,[11] suggesting that DSC can be used to determine whether the two grafted polymers in the mixed brush layer are microphase separated or not. Figure 3 shows the DSC thermograms of five HDMB samples along with the corresponding high density P*t*BA hairy particles. All particles were thermally annealed at 120 °C in vacuum for 3 h prior to the DSC analysis. For P*t*BA hairy particles, the glass transition occurred in the temperature range of 33−51 °C with the middle point at 44 °C (thermogram **1**), which was essentially the same as that of P*t*BA brushes grafted on 180 nm silica particles with P*t*BA M_n of 24.2 kDa and grafting density of 0.40 chains/nm^2 and was 10 °C higher than that of a free P*t*BA with M_n of 24.2 kDa.[11] This is believed to be caused by the surface tethering effect as discussed by Savin et al.[22] All five mixed brush samples exhibited two glass transitions with the middle points at 47−51 and 79−94 °C, which corresponded to the glass transitions of P*t*BA and PS, respectively, indicating that the two grafted polymers were microphase separated in the brush layer. Note that the PS glass transition of particle **I-1** was quite weak, but still discernible.

By carefully examining the DSC thermograms in Figure 3, we can find three trends for the two glass transitions. First, with the increase of PS molecular weight from 8.7 to 28.0 kDa, the T_g of PS increased from 79 °C (particle **I-1**), to 84 °C (particle **I-2**), to 90 °C (particle **I-3**), to 93 °C (particle **I-4**), and 94 °C (particle **I-5**). This increase is believed to be mainly due to the molecular weight effect on T_g.[13,21] It has been reported in the literature that the enhancement of T_g of polymer brushes caused by end grafting becomes smaller with the increase of polymer chain length.[22] Second, the T_g of P*t*BA also increased slightly with the increase of PS chain length, from 44 °C for homopolymer P*t*BA brushes, to 47 °C (particle **I-1**), to 49 °C (particles **I-2** and **I-3**), and 51 °C (particles **I-4** and **I-5**). This is likely due to the confining effect of PS, a higher T_g polymer, on P*t*BA nanodomains. Third, the temperature range of the P*t*BA glass transition (16 °C) in particle **I-1** was similar to that of P*t*BA homopolymer brushes on silica particles (18 °C), while the transition zone became increasingly narrower with the increase of PS molecular weight from 13.4 to 28.0 kDa (Table 2). The temperature ranges of the P*t*BA glass transition for particles **I-1** to **I-5** were ∼16, 14, 14, 12, and 6 °C, respectively. On the other hand, the PS transition zone became increasingly wider, from 10 and 8 °C for particles **I-1** and **I-2**, respectively, to 18 °C for particle **I-3** and 24 °C for particles **I-4** and **I-5**. The glass transition ranges are related to the segmental mobilities of polymer chains; the variations observed in Figure 3 could result from the different nanostructures formed from microphase separation of two grafted polymers in the brush layer. For a large chain length disparity, as suggested by theoretical and simulation studies[5,6] and confirmed in our previous experimental work,[13] a two-layered nanostructure was formed, composed of a laterally microphase separated bottom layer and a thin top layer of the longer species. The longer polymer species thus had different segmental mobilities in the bottom and outer layers and consequently exhibited a broad glass transition. On the other hand, the chains of another polymer were completely wrapped by the longer species, which manifested in a narrower glass transition zone. Evidently, this is the case for particle **I-1** in which DP_{PS}/DP_{PtBA} was 0.59 and for particles **I-3** to **I-5** in which the ratios of DP_{PS} to DP_{PtBA} were 1.31, 1.70, and 1.88, respectively. Particle **I-2** was in between these extremes (DP_{PS}/DP_{PtBA} = 0.90), and the two grafted polymers were likely to self-assemble into a "rippled" morphology.

Phase Morphologies of High Grafting Density Asymmetric Mixed P*t*BA/PS Brushes on Silica Particles. For TEM study of phase morphologies of mixed P*t*BA/PS brushes, the particles were dispersed in $CHCl_3$, a good solvent for both P*t*BA and PS, drop-cast onto carbon-coated TEM grids, and then annealed with $CHCl_3$ vapor in a closed jar for at least 3 h. The samples were stained with RuO_4 at room temperature for 20 min and then examined under a transmission electron

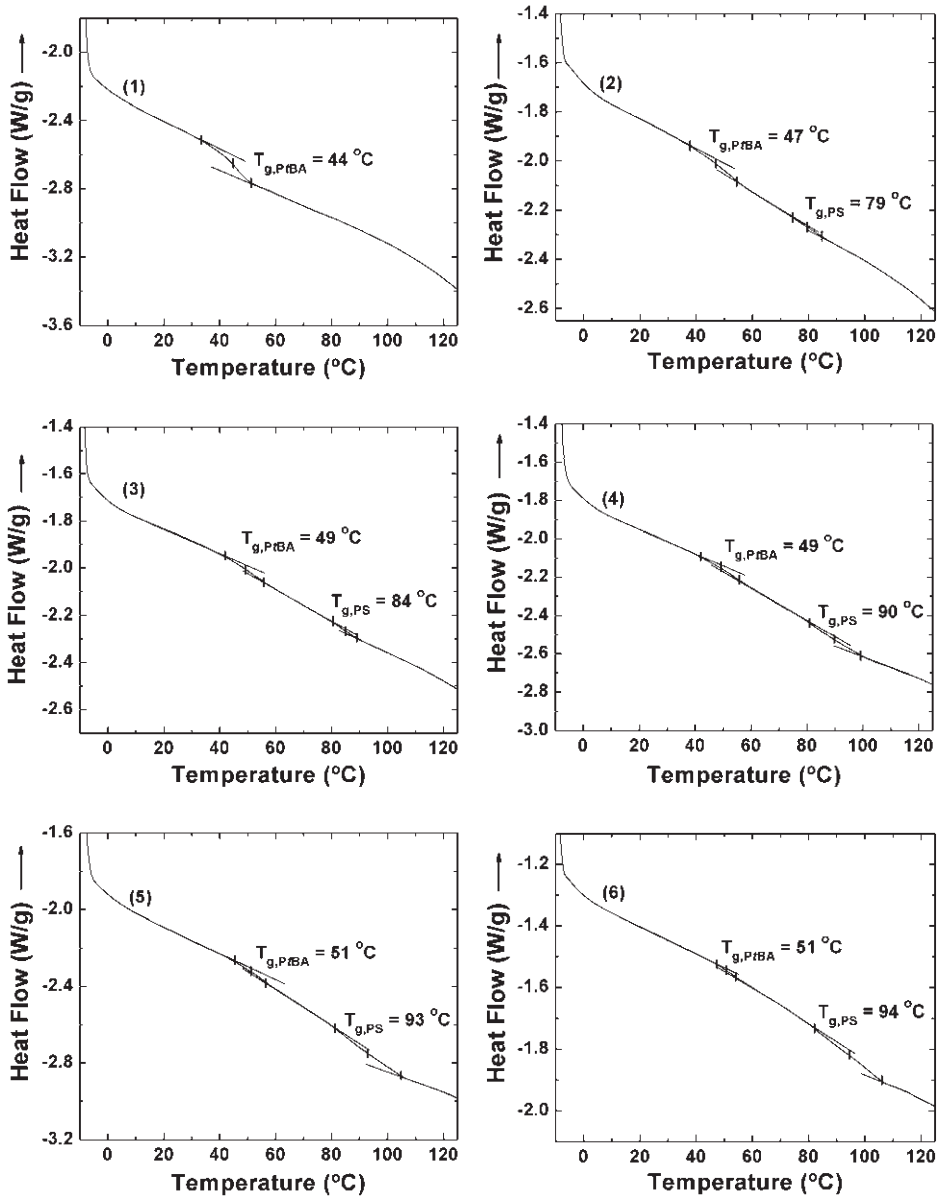

Figure 3. Differential scanning calorimetry (DSC) analysis of (1) P*t*BA brush-grafted silica particles (P*t*BA M_n = 18.6 kDa), (2) particle **I-1** (P*t*BA M_n = 18.6 kDa and PS M_n = 8.7 kDa), (3) particle **I-2** (P*t*BA M_n = 18.6 kDa and PS M_n = 13.4 kDa), (4) particle **I-3** (P*t*BA M_n = 18.6 kDa and PS M_n = 19.4 kDa), (5) particle **I-4** (P*t*BA M_n = 18.6 kDa and PS M_n = 25.3 kDa), and (6) particle **I-5** (P*t*BA M_n = 18.6 kDa and PS M_n = 28.0 kDa). The heating and cooling rates in the DSC analysis were 10 °C/min.

Table 2. Glass Transitions of High Grafting Density Homopolymer P*t*BA Brushes and High Grafting Density Mixed P*t*BA/PS Brushes on Silica Particles

sample	DP_{PS}/DP_{PtBA} [b]	$T_{g,PtBA}$ (°C)[c]	temp range of P*t*BA glass transition (°C)[c]	$T_{g,PS}$ (°C)[c]	temp range of PS glass transition (°C)[c]
P*t*BA particles[a]	0	44	33−51	NA	NA
particle **I-1**	0.59	47	38−54	79	74−84
particle **I-2**	0.90	49	41−55	84	80−88
particle **I-3**	1.31	49	42−56	90	81−99
particle **I-4**	1.70	51	45−57	93	81−105
particle **I-5**	1.88	51	48−54	94	82−106

[a] P*t*BA brush-grafted silica particles with P*t*BA M_n of 18.6 kDa; the grafting density of P*t*BA (σ_{PtBA}) = 0.63 chains/nm^2. [b] The ratio of degree of polymerization (DP) of PS to that of P*t*BA. [c] The glass transition temperature (T_g) and the temperature range of glass transition were estimated from DSC thermograms in Figure 3. There could be an error of ±1 °C.

microscope. Note that RuO_4 stains PS chains, making PS and P*t*BA nanodomains appear dark and bright, respectively, under the electron microscope.[11−13] Without RuO_4 staining, the nanostructures formed from microphase separation of mixed P*t*BA/PS brushes cannot be seen.[11] Figure 4 shows the typical top-view TEM micrographs of five HDMB samples (particles **I-1** to **I-5**).[23] For comparison, the representative TEM images of particles **II-1** to **II-4** are presented in Figure 5 (the TEM samples of particles **II-1** to **II-4** were prepared using the same procedure for HDMB samples).[23]

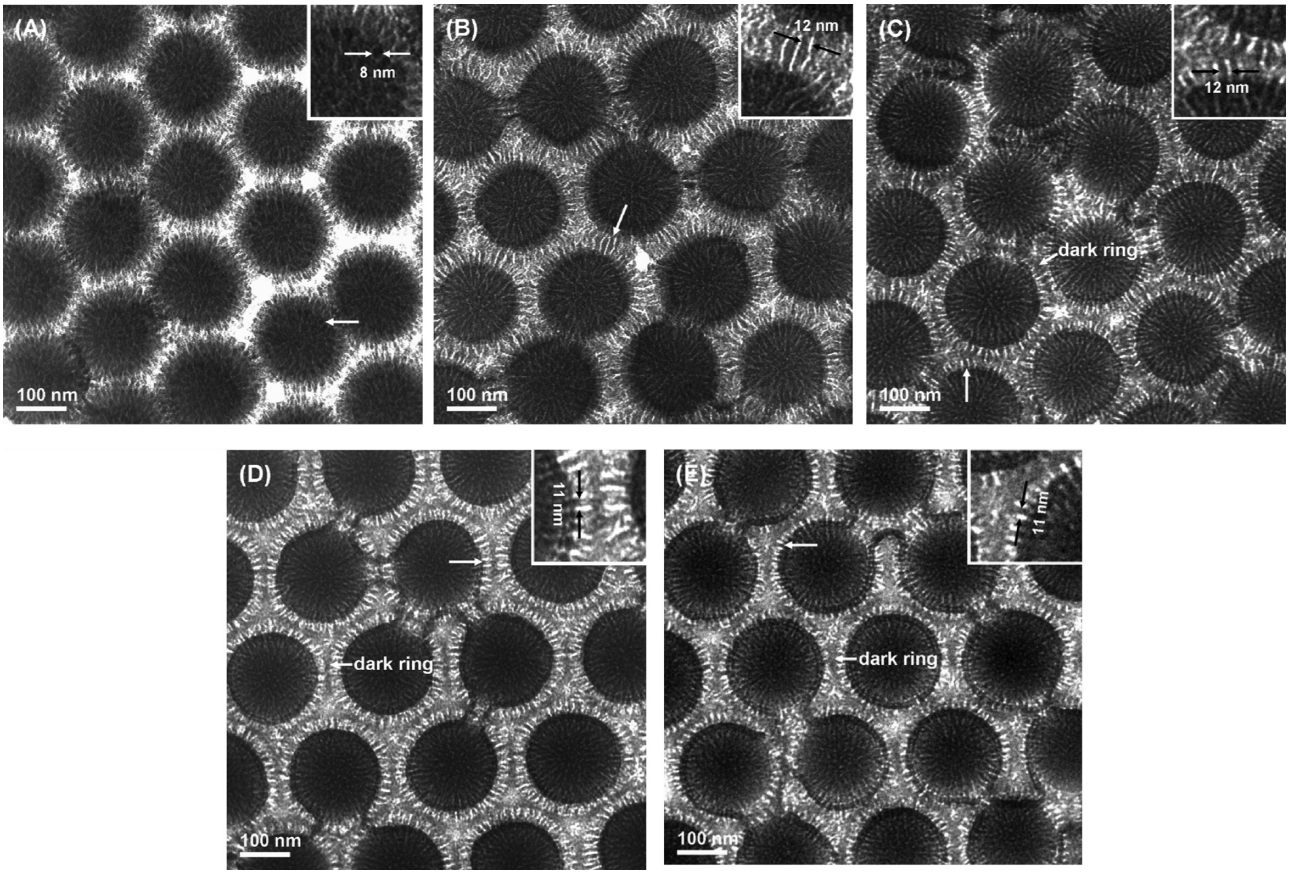

Figure 4. Top-view bright field TEM micrographs of (A) particle **I-1** (P*t*BA M_n = 18.6 kDa, σ_{PtBA} = 0.63 chains/nm^2; PS M_n = 8.7 kDa, σ_{PS} = 0.26 chains/nm^2; DP_{PS}/DP_{PtBA} = 0.59), (B) particle **I-2** (P*t*BA M_n = 18.6 kDa, σ_{PtBA} = 0.63 chains/nm^2; PS M_n = 13.4 kDa, σ_{PS} = 0.33 chains/nm^2; DP_{PS}/DP_{PtBA} = 0.90), (C) particle **I-3** (P*t*BA M_n = 18.6 kDa, σ_{PtBA} = 0.63 chains/nm^2; PS M_n = 19.4 kDa, σ_{PS} = 0.43 chains/nm^2; DP_{PS}/DP_{PtBA} = 1.31), (D) particle **I-4** (P*t*BA M_n = 18.6 kDa, σ_{PtBA} = 0.63 chains/nm^2; PS M_n = 25.3 kDa, σ_{PS} = 0.56 chains/nm^2; DP_{PS}/DP_{PtBA} = 1.70), and (E) particle **I-5** (P*t*BA M_n = 18.6 kDa, σ_{PtBA} = 0.63 chains/nm^2; PS M_n = 28.0 kDa, σ_{PS} = 0.58 chains/nm^2; DP_{PS}/DP_{PtBA} = 1.88) after being cast from a $CHCl_3$ dispersion and annealed with $CHCl_3$ vapor ($CHCl_3$ is a good solvent for both P*t*BA and PS). The samples were stained with RuO_4 vapor at room temperature for 20 min. The inset in each TEM micrograph shows the enlarged area marked by the long white arrow.

Clearly, all high grafting density mixed brushes were microphase separated, consistent with the DSC results. Moreover, the morphology varied with the increase of the PS molecular weight. By comparing the TEM micrographs in Figures 4 and 5, one can easily find out that the grafting density has a significant effect on the self-assembled nanostructures of mixed brushes, particularly, the feature size. For particle **I-1** in which the PS M_n (8.7 kDa) was significantly lower than that of P*t*BA (18.6 kDa, DP_{PS}/DP_{PtBA} = 0.59), the PS chains self-assembled into irregular, mostly isolated nanodomains with a typical width of around 8 nm (the nanodomain pointed by arrows in Figure 4A and its inset; see the illustrated nanostructure in Scheme 2a). This is similar to the morphology of particle **II-1** (PS M_n = 14.8 kDa; DP_{PS}/DP_{PtBA} = 0.74) where PS segregated into isolated nanodomains with a typical width of 13 nm (the nanodomain pointed by arrows in Figure 5A and its inset). Different from Figure 5A, the dark PS nanodomains in particle **I-1** were denser and smaller. The smaller size is believed to mainly result from the higher overall grafting density (σ_{total} = 0.89 chains/nm^2 in particle **I-1** and 0.57 chains/nm^2 in particle **II-1**), though the difference in PS molecular weight may also contribute. Note that the root-mean-square end-to-end distances $\langle R_{rms} \rangle$ of PS with molecular weight of 8.7 and 14.8 kDa in the unperturbed state are 6.2 and 8.0 nm (Table 1), respectively. The PS in particle **II-2** was slightly longer than that in particle **II-1**; short cylinders with a typical width of 13 nm were observed (the nanodomain pointed by arrows in Figure 5B and its inset).

For particle **I-2** in which the chain lengths of two polymers were very close to each other (DP_{PtBA} = 143 and DP_{PS} = 129), the two grafted polymers underwent lateral microphase separation, producing a "rippled" nanostructure (Figure 4B), though there was a difference in the grafting densities of two polymers (σ_{PtBA} = 0.63 chains/nm^2; σ_{PS} = 0.33 chains/nm^2). Note that simulation studies have suggested that the cocontinuous "rippled" morphology can tolerate small chain length and grafting density asymmetries.[5,6] The polymer chains spread out and covered the interstitial space among neighboring particles. Interestingly, the dark and bright stripes from one particle were connected to those from neighboring particles, forming alternating bridging nanodomains (marked by an arrow in Figure 4B). No dark or bright thin layer was observed at the boundary of neighboring hairy particles, suggesting that the nanostructure was simply a "rippled" phase with no thin layer of a pure species on the top (Scheme 2B). This is consistent with the DSC result for this sample, where relatively narrow glass transitions were observed for both grafted polymers. The width of a typical PS stripe and the ripple wavelength (pointed by the arrows in Figure 4B and its inset) on the particles were estimated to be 8 and 12 nm, respectively. This sample resembles particle **II-3** in which the two grafted polymers self-assembled into a "rippled" nanostructure (Figure 5C). However, the feature size of particle **II-3** is significantly larger with the PS stripe width of 15 nm and the ripple wavelength of 20 nm (the PS and P*t*BA stripes pointed by the arrows in Figure 5C and its inset).

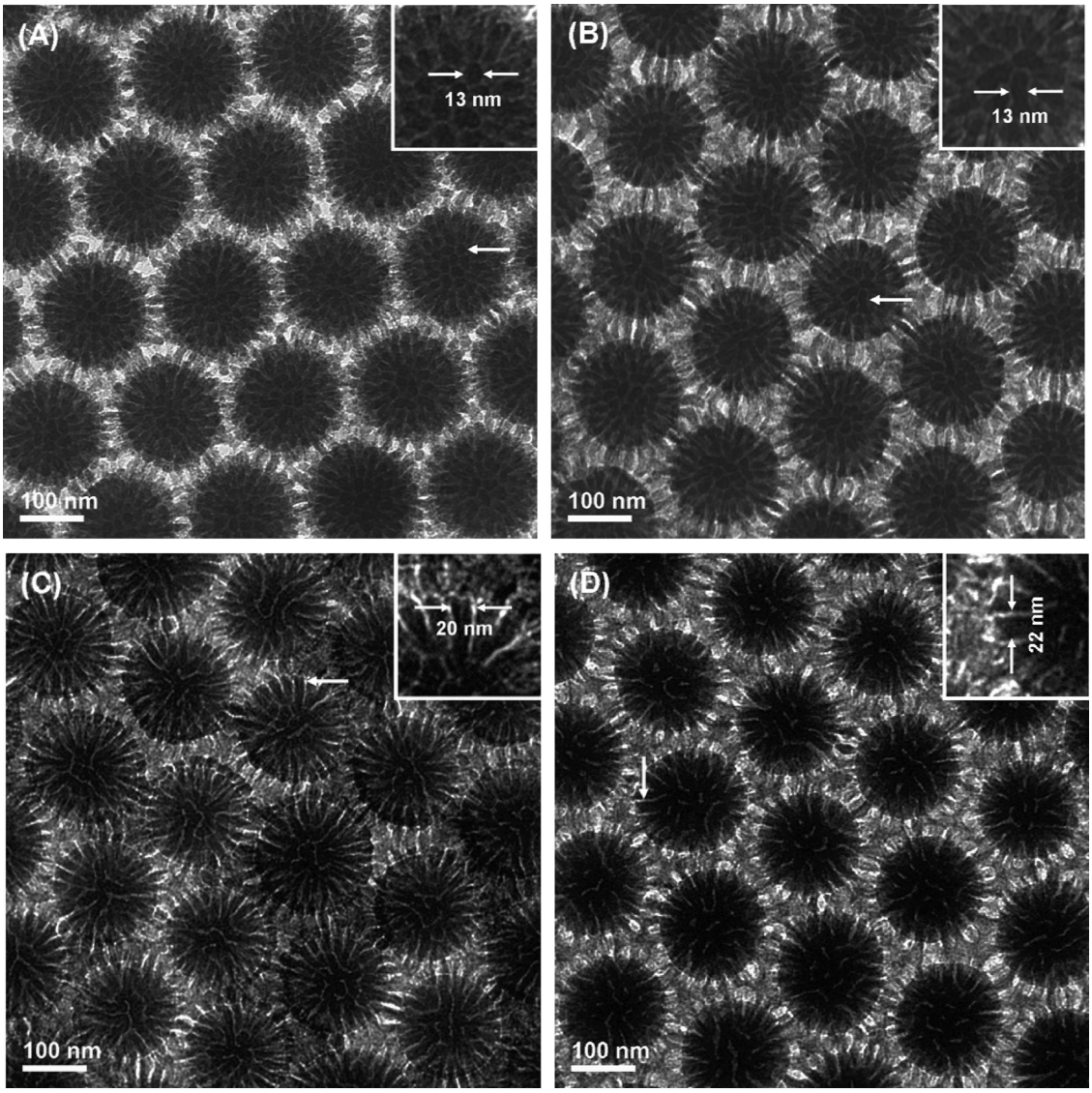

Figure 5. Top-view bright field TEM micrographs of (A) particle **II-1** (P*t*BA M_n = 24.5 kDa, σ_{PtBA} = 0.36 chains/nm^2; PS M_n = 14.8 kDa, σ_{PS} = 0.21 chains/nm^2; DP_{PS}/DP_{PtBA} = 0.74), (B) particle **II-2** (P*t*BA M_n = 24.5 kDa, σ_{PtBA} = 0.36 chains/nm^2; PS M_n = 18.7 kDa, σ_{PS} = 0.26 chains/nm^2; DP_{PS}/DP_{PtBA} = 0.94), (C) particle **II-3** (P*t*BA M_n = 24.5 kDa, σ_{PtBA} = 0.36 chains/nm^2; PS M_n = 24.9 kDa, σ_{PS} = 0.27 chains/nm^2; DP_{PS}/DP_{PtBA} = 1.25), and (D) particle **II-4** (P*t*BA M_n = 24.5 kDa, σ_{PtBA} = 0.36 chains/nm^2; PS M_n = 30.4 kDa, σ_{PS} = 0.32 chains/nm^2; DP_{PS}/DP_{PtBA} = 1.53) after being cast from a $CHCl_3$ dispersion and annealed with $CHCl_3$ vapor ($CHCl_3$ is a good solvent for both P*t*BA and PS). The samples were stained with RuO_4 vapor at room temperature for 20 min. The inset in each TEM micrograph shows the enlarged area marked by the white arrow.

Scheme 2. Schematic Illustration of Microphase Separation of High Density Mixed P*t*BA/PS Brushes with P*t*BA M_n (a) Higher Than, (b) Comparable to, and (c) Lower Than That of PS M_n

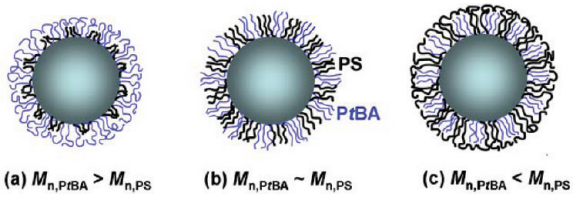

For particle **I-3** in which the chain length of PS (DP = 187) was slightly longer than that of P*t*BA (DP = 143) and the grafting densities of two polymers were comparable (σ_{PtBA} = 0.63 chains/nm^2; σ_{PS} = 0.43 chains/nm^2), the morphology (Figure 4C) is quite similar to that of particle **I-2** (Figure 4B), but there is a difference. A dark layer appeared in the interstitial area between the particles and each particle was surrounded by a nearly continuous "ring" of such a dark layer (marked by a short arrow in Figure 4C). This suggests that the two grafted polymers microphase separated into a two-layered nanostructure in which the bottom layer was laterally microphase separated and covered by a thin PS top layer because the PS chains were slightly longer than that of P*t*BA (Scheme 2c). The typical width of dark PS nanodomains and the typical periodicity in the bottom layer, pointed by the long arrows, were 8 and 12 nm, respectively, which were significantly smaller than those of particle **II-3** (15 and 20 nm, respectively). Note that the $\langle R_{rms} \rangle$ of PS with M_n of 19.4 kDa in the unperturbed state is 9.2 nm (Table 1), only slightly smaller than that of PS with M_n of 24.9 kDa (10.4 nm), which cannot explain the observed much smaller feature size. The higher overall grafting density appears to be responsible for the observation. From Figure 4C, the PS and P*t*BA nanodomains that were underneath the thin PS layer appeared to be mostly cylindrical. Note that the ratios of DP_{PS} to DP_{PtBA} and σ_{PS} to σ_{PtBA} in

particle **II-3** were almost the same as those in particle **I-3**, but dark rings in Figure 5C were not as visible and defined as in Figure 4C. We speculate that at lower grafting densities the PS nanodomains formed from lateral microphase separation can accommodate more PS segments, while at higher grafting densities the polymer chains are more stretched, resulting in the formation of a thin PS top layer. The distribution of PS segments in two layers is presumably the origin of the broader PS glass transition of particle **I-3** compared with those of particles **I-1** and **I-2** (Figure 3).

For particles **I-4** and **I-5** where the grafting densities of two polymers were very close to one another and the PS chain length was significantly longer than that of P*t*BA, two-layered nanostructures were formed as in particle **I-3** and composed of a microphase-separated bottom layer and a dark PS top layer. The dark rings became thicker with the increase of PS molecular weight (Figure 4D,E). Moreover, compared with the bottom layer in particle **I-3**, the P*t*BA nanodomains became increasingly isolated. The typical width of PS nanodomains and the periodicity were 7 and 11 nm, respectively, in particle **I-4** and 6 and 11 nm, respectively, in particle **I-5** (marked by long arrows). These values are significantly smaller than those observed in particle **II-4** (17 and 22 nm, respectively). Note that the ratios of DP_{PS} to DP_{PtBA} and σ_{PS} to σ_{PtBA} were all similar for particles **I-4**, **I-5**, and **II-4** (Table 1) and the dark rings can also be seen in the TEM image of particle **II-4** (Figure 5D). The difference in the overall grafting density appears to be responsible for the observed feature size differences.

We previously reported self-assembled nanostructures of particles **II-1** to **II-4** after thermal annealing at 120 °C, which was above the glass transition temperatures of PS and P*t*BA.[13] The phase morphology evolution was the same as observed here for the particles after being cast and annealed with $CHCl_3$ vapor. However, compared with the morphology of the same sample after thermal annealing, the width of PS nanodomains here was slightly larger; the PS nanodomains look slightly "swollen", especially for particle **II-4** (Figure 5D). This observation could be due to the following reasons. (i) $CHCl_3$ is a good solvent for both PS and P*t*BA. Theoretical studies have suggested that the microphase separation of mixed brushes in a nonselective solvent may be delayed with improving the solvent quality.[4b] We speculate that the interfacial layer between PS and P*t*BA nanodomains was thicker and RuO_4 also stained the interfacial layer. (ii) The solubility parameter of $CHCl_3$ is 9.3 $(cal/cm^3)^{0.5}$.[21] Using the group molar attraction constants and molar volume constants from a textbook,[24] we calculated the solubility parameters of PS and P*t*BA and they were 9.5 and 8.5 $(cal/cm^3)^{0.5}$, respectively. Thus, $CHCl_3$ is a slightly better solvent for PS than for P*t*BA and it could slightly preferentially swell PS during the solvent casting and annealing processes, making PS nandomain width slightly larger.

The DP of P*t*BA in HDMB was 143, lower than that of P*t*BA in IDMB (DP = 191). To further confirm that the observed much smaller feature sizes in Figure 4 were mainly due to the higher total grafting densities, not the molecular weight differences between the polymers in HDMB and IDMB, we synthesized another high density mixed P*t*BA/PS brush sample (particle **III-1** in Table 1).[16] The values of P*t*BA M_n, DP, and PDI were 23.7 kDa, 189, and 1.09, respectively, while the M_n, DP, and PDI of PS were 25.7 kDa, 247, and 1.14, respectively. The $\langle R_{rms} \rangle$s of free P*t*BA and PS, corresponding to particle **III-1**, in the unperturbed state are essentially identical to those corresponding to particle **II-3** (Table 1). The calculated grafting densities of P*t*BA and PS were 0.48 and 0.51 chains/nm^2. DSC analysis showed that the two polymers were microphase separated.[20] A morphology similar to those in Figure 4C−E was observed, i.e., a two-layered nanostructure composed of a laterally microphase-separated bottom layer and a thin PS top layer (Figure 6).[23] The width of a typical PS nanodomain and the periodicity in the bottom layer marked by the long arrows were 8 and 13 nm, respectively, which were similar to those in Figure 4C. This confirmed that the observed much smaller feature sizes in Figure 4 indeed resulted from the higher total grafting densities. It can be imagined that at high grafting densities polymer chains are highly stretched, which means that the entropy of polymer chains is considerably lower compared with that in IDMB. Consequently, the lateral microphase separation is restricted to a smaller lateral dimension as any further stretching of polymer chains in the lateral direction would further decrease the entropy, which may not be compensated by the energy gain from lateral microphase separation.

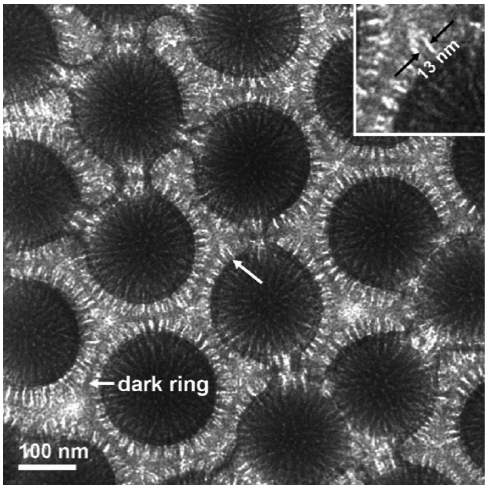

Figure 6. Top-view bright field TEM micrograph of particle **III-1** (P*t*BA M_n = 23.7 kDa, σ_{PtBA} = 0.48 chains/nm^2; PS M_n = 25.7 kDa, σ_{PS} = 0.51 chains/nm^2; DP_{PS}/DP_{PtBA} = 1.31) after being cast from a $CHCl_3$ dispersion and annealed with $CHCl_3$ vapor ($CHCl_3$ is a good solvent for both P*t*BA and PS). The sample was stained with RuO_4 vapor at room temperature for 20 min. The inset on the top right corner shows the enlarged area marked by the long white arrow.

Conclusions

We synthesized a series of high density asymmetric mixed P*t*BA/PS brushes with a fixed P*t*BA M_n of 18.6 kDa and PS molecular weight ranging from 8.7 to 28.0 kDa from 172 nm Y-initiator-functionalized silica particles by sequential ATRP and NMRP. The Y-initiator particles were prepared from bare silica particles by using a triethoxysilane-terminated Y-initiator via a hydrolysis/condensation process in the presence of ammonia. The total grafting densities of the obtained mixed P*t*BA/PS brushes were in the range of 0.9−1.2 chains/nm^2, which were significantly larger than those of IDMB synthesized from monochlorosilane-terminated Y-initiator-functionalized silica particles (0.6−0.7 chains/nm^2). DSC analysis suggested that all HDMB were microphase separated. TEM showed that the phase morphology of these mixed brushes evolved from mostly isolated PS nanodomains in the P*t*BA matrix to a nearly cocontinuous, wormlike nanostructure and two-layered nanostructures composed of a laterally microphase-separated bottom layer and a thin top layer of the longer polymer chains with the increase of PS molecular weight from below to above that of P*t*BA. This observation is similar to that of intermediate density mixed brushes with total grafting densities of 0.6−0.7 chains/nm^2.

However, the feature sizes of the patterns formed from microphase separation of HDMB were significantly smaller than those of IDMB, which was attributed to the difference in total grafting density. In HDMB, polymer chains are much more stretched than those in IDMB. As a result, the lateral microphase separation occurred in a smaller lateral dimension because splaying of polymer chains to any larger extent in the lateral direction would further decrease the entropy, which is not compensated by the energy gain from lateral microphase separation. This is the first time that the effect of grafting density on phase morphology of mixed brushes was directly observed by TEM. The results reported in this article could allow us to better use mixed brushes in the design and fabrication of novel nanostructured materials for future technological uses.

Acknowledgment. B.Z. thanks the University of Tennessee and NSF (DMR-0906913 and -1007986) for the support of this work. L.Z. thanks NSF (DMR-1007918) for financial support. Parts of this work were carried out in the Characterization Facility of the College of Science and Engineering, University of Minnesota, which receives partial support from NSF through the MRSEC program. B.Z. thanks the MRSEC of the University of Minnesota for providing Materials Research Facilities Network (MRFN) funding for using TEM at University of Minnesota.

Supporting Information Available: Experimental section including the synthesis of Y-initiator particles, synthesis of high grafting density P*t*BA brushes and mixed P*t*BA/PS brushes, and the detailed procedures for DSC and TEM experiments; SEC traces of five polymers formed from STEMPO in the synthesis of mixed P*t*BA/PS brush-grafted silica particles from P*t*BA brush-grafted particles with P*t*BA M_n of 18.6 kDa by surface-initiated NMRP; top-view bright field TEM micrographs of particles **I-1** to **I-5** and particles **II-1** to **II-4**; TGA of particle **III-1**; DSC analysis of particle **III-1**; top-view bright field TEM micrographs of particle **III-1**. This material is available free of charge via the Internet at http://pubs.acs.org.

References and Notes

(1) (a) Marko, J. F.; Witten, T. A. *Phys. Rev. Lett.* **1991**, *66*, 1541–1544. (b) Marko, J. F.; Witten, T. A. *Macromolecules* **1992**, *25*, 296–307. (c) Dong, H. *J. Phys. II* **1993**, *3*, 999–1020. (d) Brown, G.; Chakrabarti, A.; Marko, J. F. *Europhys. Lett.* **1994**, *25*, 239–244. (e) Luzinov, I.; Minko, S.; Tsukruk, V. V. *Prog. Polym. Sci.* **2004**, *29*, 635–698. (f) Luzinov, I.; Minko, S.; Tsukruk, V. V. *Soft Matter* **2008**, *4*, 714–725. (g) Zhao, B.; Brittain, W. J. *Prog. Polym. Sci.* **2000**, *25*, 677–710.

(2) Zhao, B.; Zhu, L. *Macromolecules* **2009**, *42*, 9369–9383.

(3) Zhulina, E.; Balazs, A. C. *Macromolecules* **1996**, *29*, 2667–2673.

(4) (a) Lai, P. Y. *J. Chem. Phys.* **1994**, *100*, 3351–3357. (b) Soga, K. G.; Zuckermann, M. J.; Guo, H. *Macromolecules* **1996**, *29*, 1998–2005. (c) Singh, C.; Pickett, G. T.; Balazs, A. C. *Macromolecules* **1996**, *29*, 7559–7570. (d) Müller, M. *Phys. Rev. E* **2002**, *65*, 030802. (e) Minko, S.; Müller, M.; Usov, D.; Scholl, A.; Froeck, C.; Stamm, M. *Phys. Rev. Lett.* **2002**, *88*, 035502. (f) Wenning, L.; Müller, M.; Binder, K. *Europhys. Lett.* **2005**, *71*, 639–645. (g) Merlitz, H.; He, G. L.; Sommer, J. U.; Wu, C. X. *Macromolecules* **2009**, *42*, 445–451.

(5) Roan, J.-R. *Phys. Rev. Lett.* **2006**, *96*, 248301.

(6) Wang, J.; Müller, M. *J. Phys. Chem. B* **2009**, *113*, 11384–11402.

(7) (a) Sidorenko, A.; Minko, S.; Schenk-Meuser, K.; Duschner, H.; Stamm, M. *Langmuir* **1999**, *15*, 8349–8355. (b) Minko, S.; Usov, D.; Goreshnik, E.; Stamm, M. *Macromol. Rapid Commun.* **2001**, *22*, 206–211. (c) Motornov, M.; Minko, S.; Eichhorn, K. J.; Nitschke, M.; Simon, F.; Stamm, M. *Langmuir* **2003**, *19*, 8077–8085. (d) Lemieux, M.; Usov, D.; Minko, S.; Stamm, M.; Shulha, H.; Tsukruk, V. V. *Macromolecules* **2003**, *36*, 7244–7255. (e) Usov, D.; Gruzdev, V.; Nitschke, M.; Stamm, M.; Hoy, O.; Luzinov, I.; Tokarev, I.; Minko, S. *Macromolecules* **2007**, *40*, 8774–8783. (f) Santer, S.; Kopyshev, A.; Yang, H. K.; Rühe, J. *Macromolecules* **2006**, *39*, 3056–3064.

(8) (a) Minko, S.; Patil, S.; Datsyuk, V.; Simon, F.; Eichhorn, K. J.; Motornov, M.; Usov, D.; Tokarev, I.; Stamm, M. *Langmuir* **2002**, *18*, 289–296. (b) Minko, S.; Müller, M.; Motornov, M.; Nitschke, M.; Grundke, K.; Stamm, M. *J. Am. Chem. Soc.* **2003**, *125*, 3896–3900. (c) Minko, S.; Luzinov, I.; Luchnikov, V.; Müller, M.; Patil, S.; Stamm, M. *Macromolecules* **2003**, *36*, 7268–7279. (d) Ionov, L.; Minko, S.; Stamm, M.; Gohy, J. F.; Jerome, R.; Scholl, A. *J. Am. Chem. Soc.* **2003**, *125*, 8302–8306. (d) Ionov, L.; Sidorenko, A.; Stamm, M.; Minko, S.; Zdyrko, B.; Klep, V.; Luzinov, I. *Macromolecules* **2004**, *37*, 7421–7423. (e) LeMieux, M. C.; Julthongpiput, D.; Bergman, K. N.; Cuong, P. D.; Ahn, H. S.; Lin, Y. H.; Tsukruk, V. V. *Langmuir* **2004**, *20*, 10046–10054. (f) Wang, J.; Kara, S.; Long, T. E.; Ward, T. C. *J. Polym. Sci., Polym. Chem.* **2000**, *38*, 3742–3750. (g) Julthongpiput, D.; Lin, Y. H.; Teng, J.; Zubarev, E. R.; Tsukruk, V. V. *Langmuir* **2003**, *19*, 7832–7836. (h) Tsujii, Y.; Ohno, K.; Yamamoto, S.; Goto, A.; Fukuda, T. *Adv. Polym. Sci.* **2006**, *197*, 1–45. (i) Ionov, L.; Houbenov, N.; Sidorenko, A.; Stamm, M.; Luzinov, I.; Minko, S. *Langmuir* **2004**, *20*, 9916–9919. (j) Ionov, L.; Sidorenko, A.; Stamm, M.; Minko, S.; Zdyrko, B.; Klep, V.; Luzinov, I. *Macromolecules* **2004**, *37*, 7421–7423. (k) Motornov, M.; Sheparovych, R.; Tokarev, I.; Roiter, Y.; Minko, S. *Langmuir* **2007**, *23*, 13–19.

(9) (a) Zhao, B. *Polymer* **2003**, *44*, 4079–4083. (b) Zhao, B. *Langmuir* **2004**, *20*, 11748–11755. (c) Zhao, B.; He, T. *Macromolecules* **2003**, *36*, 8599–8602. (d) Zhao, B.; Haasch, R. T.; MacLaren, S. *J. Am. Chem. Soc.* **2004**, *126*, 6124–6134. (e) Zhao, B.; Haasch, R. T.; MacLaren, S. *Polymer* **2004**, *45*, 7979–7988. (f) Li, D. J.; Sheng, X.; Zhao, B. *J. Am. Chem. Soc.* **2005**, *127*, 6248–6256. (g) Santer, S.; Kopyshev, A.; Donges, J.; Rühe, J.; Jiang, X. G.; Zhao, B.; Müller, M. *Langmuir* **2007**, *23*, 279–285.

(10) (a) Chiu, J. J.; Kim, B. J.; Kramer, E. J.; Pine, D. J. *J. Am. Chem. Soc.* **2005**, *127*, 5036–5037. (b) Shan, J.; Nuopponen, M.; Jiang, H.; Viitala, T.; Kauppinen, E.; Kontturi, K.; Tenhu, H. *Macromolecules* **2005**, *38*, 2918–2926. (c) Zubarev, E. R.; Xu, J.; Sayyad, A.; Gibson, J. D. *J. Am. Chem. Soc.* **2006**, *128*, 4958–4959. (d) Guo, Y.; Moffitt, M. G. *Macromolecules* **2007**, *40*, 5868–5878. (e) Cheng, J.; He, J.; Li, C.; Yang, Y. *Chem. Mater.* **2008**, *20*, 4224–4230. (f) Motornov, M.; Sheparovych, R.; Lupitskyy, R.; MacWilliams, E.; Hoy, O.; Luzinov, I.; Minko, S. *Adv. Funct. Mater.* **2007**, *17*, 2307–2314. (g) Motornov, M.; Sheparovych, R.; Lupitskyy, R.; MacWilliams, E.; Minko, S. *J. Colloid Interface Sci.* **2007**, *310*, 481–488.

(11) Zhao, B.; Zhu, L. *J. Am. Chem. Soc.* **2006**, *128*, 4574–4575.

(12) Zhu, L.; Zhao, B. *J. Phys. Chem. B* **2008**, *112*, 11529–11536.

(13) Jiang, X. M.; Zhong, G. J.; Horton, J. M.; Jin, N. X.; Zhu, L.; Zhao, B. *Macromolecules* **2010**, *43*, 5387–5395.

(14) (a) Ohno, K.; Morinaga, T.; Koh, K.; Tsujii, Y.; Fukuda, T. *Macromolecules* **2005**, *38*, 2137–2142. (b) Ohno, K.; Morinaga, T.; Takeno, S.; Tsujii, Y.; Fukuda, T. *Macromolecules* **2006**, *39*, 1245–1249.

(15) (a) Hawker, C. J.; Bosman, A. W.; Harth, E. *Chem. Rev.* **2001**, *101*, 3661–3688. (b) Dao, J.; Benoit, D.; Hawker, C. J. *J. Polym. Sci., Part A: Polym. Chem.* **1998**, *36*, 2161–2167. (c) Zhao, B.; Jiang, X. M.; Li, D. J.; Jiang, X. G.; O'Lenick, T. G.; Li, B.; Li, C. Y. *J. Polym. Sci., Part A: Polym. Chem.* **2008**, *46*, 3438–3446.

(16) See Experimental Section in the Supporting Information.

(17) (a) Philipse, A. P.; Vrij, A. *J. Colloid Interface Sci.* **1989**, *128*, 121–136. (b) Bogush, G. H.; Tracy, M. A.; Zukoski, C. F., IV *J. Non-Cryst. Solids* **1988**, *104*, 95–106. (c) Li, D. J.; Jones, G. L.; Dunlap, J. R.; Hua, F. J.; Zhao, B. *Langmuir* **2006**, *22*, 3344–3351. (d) Li, D. J.; Zhao, B. *Langmuir* **2007**, *23*, 2208–2217. (e) Jiang, X. M.; Wang, B. B.; Li, C. Y.; Zhao, B. *J. Polym. Sci., Part A: Polym. Chem.* **2009**, *47*, 2853–2870. (c) Ohno, K.; Morinaga, T.; Takeno, S.; Tsujii, Y.; Fukuda, T. *Macromolecules* **2007**, *40*, 9143–9150.

(18) He, T.; Li, D. J.; Sheng, X.; Zhao, B. *Macromolecules* **2004**, *37*, 3128–3135.

(19) Husseman, M.; Malmstrom, E. E.; McNamara, M.; Mate, M.; Mecerreyes, D.; Benoit, D. G.; Hedrick, J. L.; Mansky, P.; Huang, E.; Russell, T. P.; Hawker, C. J. *Macromolecules* **1999**, *32*, 1424–1431.

(20) The data can be found in the Supporting Information.

(21) Hiemenz, P. C.; Lodge, T. P. *Polymer Chemistry*, 2nd ed.; CRC Press: Boca Raton, FL, 2007.

(22) Savin, D. A.; Pyun, J.; Patterson, G. D.; Kowalewski, T.; Matyjaszewski, K. *J. Polym. Sci., Part B: Polym. Phys.* **2002**, *40*, 2667–2676.

(23) More TEM micrographs can be found in the Supporting Information.

(24) Coleman, M. M.; Painter, P. C. *Fundamentals of Polymer Science: An Introductory Textbook*, 2nd ed.; CRC Press: Boca Raton, FL, 1998.